Interfacial behavior of lipid nanocapsules spread on model membrane monolayers

Tzvetanka Ivanova, Kristina Mircheva, K. Balashev, I. Minkov, Patrick
Saulnier, Ivan Panaiotov

ORIGINAL CONTRIBUTION

Interfacial behavior of lipid nanocapsules spread on model membrane monolayers

**Tz Ivanova · K. Mircheva · K. Balashev · I. Minkov ·
P. Saulnier · I. Panaiotov**

Abstract The lipid nanocapsules (LNCs) spread at the air–water interface (A/W) undergo destabilization and disaggregation leading to formation of a triglyceride (TG) surface film. The kinetics of reorganization and formation of TG surface film were followed by measuring either the change of surface pressure at constant area or the surface area at constant surface pressure. From the obtained experimental data were determined the effectiveness of TG spreading and the rate of LNC disaggregation at A/W interface covered with preformed model membrane monolayers of DPPC, Curosurf®, and mucus. Partial LNC stabilization due to their interaction with the model membrane monolayers was observed and characterized by atomic force microscopy (AFM). The obtained results demonstrated that the LNCs spread on mucus surface layer, which models the epithelial surface were more stable than if they were spread either on DPPC or Curosurf® surface layers, which emulate the alveolar surface.

Abbreviations

LNCs	Lipid nanocapsules
TG	Triglyceride
Lab≡TG	Labrafac®
DPPC	Dipalmitoylphosphatidylcholine
A/W	Air–water
LS	Lung surfactant

T. Ivanova (✉) · K. Mircheva · K. Balashev · I. Minkov ·
I. Panaiotov
Biophysical Chemistry Laboratory, Dept. of Physical Chemistry,
Faculty of Chemistry and Pharmacy, University of Sofia, J.
Bourchier str. 1, 1164 Sofia, Bulgaria
e-mail: tzivanova@chem.uni-sofia.bg

P. Saulnier
INSERM U1066 MINT "Micro et Nanomédecines Biomimétiques",
LUNAM Université, 49100 Angers, France

Introduction

Over the last decade after the introduction of basic or modified lipid nanocapsules (LNCs) in pharmaceutical practice, they have been successfully utilized as effective drug delivery systems [1–6]. The basic LNCs obtained by phase-inversion method contain a triglyceride (TG) core covered by phospholipid molecules and a soft layer formed from hydroxystearate of polyethylene glycol [1, 2]. The mechanisms of destabilization and reorganization of LNCs after their spreading at pure air–water (A/W) interface were studied in various aspects whereby two populations of nanocapsules without (LNCs I) and with (LNCs II) phospholipid molecules were identified [7–10]. Both fractions were found to be stable and to remain intact in the bulk of their suspensions. A loss of mechanical stability at A/W interface was observed for the fraction without lipid molecules, which underwent rapid destabilization with a rate constant k_1 followed by disaggregation and formation of a TG surface film. It was assumed that k_1 was related to the characteristic time of interfacial disaggregation of the unstable type I nanoparticles, whereas the spreading of TG molecules confined into capsules was instantaneous.

Studying the mechanisms of loss of mechanical stability and reorganization of LNCs containing encapsulated liposoluble drugs in the processes of interaction with various model membrane systems seems appropriate for better understanding of their behavior at the cell membrane interface. Thus, using a monolayer spread at the A/W interface as a simplified convenient membrane model, three monolayer systems were chosen : (*i*) Dipalmitoylphosphatidylcholine (DPPC) monolayer mimicking the cell membrane; (*ii*) lung surfactant (LS) layer accumulated at the alveolar surface of lung; and (*iii*) pig intestinal mucus layer.

The monolayer of saturated phospholipid DPPC is largely preferred as a model of biomembrane because DPPC is the most common lipid component of cell membranes [11–15] as well as because the drug insertion into preformed DPPC monolayers is found to be alike as drug penetration via

biological membranes [16]. DPPC is also the main component of LS. The physiological contribution of LS accumulated at the alveolar surface is related to the maintenance of structural stability of the alveoli during respiration process by reducing the surface tension between alveolar lining layer and gas phase. Curosurf® is a commercially available natural LS, which contains about 70 % DPPC of total phospholipid content. It is clinically applicable in cases of LS absence in premature infants [17, 18]. Both DPPC and Curosurf® monolayers were often used as model systems of the alveolar surface. For example, the insertion of pulmonary antitubercular drug into LS monolayer has been investigated as the drug was administrated by an appropriated drug delivery system toward the model alveolar surface [19].

The epithelial surface is covered by a highly glycosylated mucus layer that serves as a physical barrier between the extracellular environment and plasma membranes [20]. Recently, the interaction of newly developed LNCs for oral delivery with pig intestinal mucus layer having thickness of several hundred microns were studied by fluorescence resonance energy transfer (FRET) method in order to improve the bioavailability of liposoluble drug Paclitaxel encapsulated in these LNCs [21]. Investigating the processes of adsorption on mucus layer also requires finding a model system where the experimental conditions and physicochemical parameters are under strict control [22, 23]. As such, the mucus monolayer at A/W interface appears to be the right candidate.

The purpose of this paper is to study the mechanisms of destabilization and reorganization of basic LNCs spread on three types preformed at the A/W interface monolayers of: DPPC, Curosurf® and pig intestinal mucus. In this approach, the monolayers of DPPC and Curosurf® served as a model of the alveolar surface and the mucus monolayer is considered as a model of the luminal surface of gastrointestinal tract. Furthermore, the monolayers studies at A/W interface were accompanied with atomic force microscopy (AFM) imaging of Langmuir–Blodgett (LB) films of the monolayer systems under investigation after their transfer from the A/W interface on mica solid supports.

Materials and methods

Materials

DPPC with a molecular weight (MW) of 734.04 was provided by Sigma-Aldrich. Labrafac® WL1349 (Lab) provided by Gattefossé S.A. (Saint- Priest, France) is a mixture of caprylic and capric acid TG with average MW=512. Lipoid® (Lip) S75-3 from Lipoid GmbH (Ludwigshafen, Germany) is a soybean lecithin with 69 % of phosphatidylcholine and an average MW=800. Solutol® HS15 (Sol) provided by BASF (Ludwigshafen, Germany) with an average MW=911 is a

mixture of free polyethylene glycol 660 (~30 %) and 12-hydroxystearate of polyethylene glycol 660 (~70 %). Curosurf® (Chiesi Farmaceutici, Parma, Italy) is a natural surfactant extract, prepared from porcine lungs, containing almost exclusively polar lipids in particular phosphatidylcholine (about 70 % of total phospholipid content), phosphatidylglycerol (about 30 % of total phospholipid content) and about 1 % of surfactant associated hydrophobic proteins SP-B and SP-C. Pig intestinal mucus containing mucin 5 %, lipids 37 %, proteins 39 %, DNA 6 % other 13 % of dry weight was prepared by the colleagues from the University of Angers (France). NaCl was a product of Theokom (Sofia, Bulgaria). Double distilled water was used in all experiments.

Considering the complex composition of each product, the brand names and their abbreviations will be used in the article.

Methods

Preparation of LNC

LNCs were prepared using the procedure described by Heurtault et al. [1, 2]. All components (Labrafac®, Lipoid®, Solutol®, NaCl, and doubly distilled water) were mixed. Three cycles of progressive heating and cooling combined with magnetic stirring at an agitation speed of 200 rpm, were performed. The first and second cycles were between 85 and 60 °C, whereas the third one was between 85 and 70 °C. When the sample temperature reached 70 °C, a fast cooling dilution was made by rapid addition of 12.5 cm³ cold (~T=0 °C) double-distilled water. After preparation of the LNC aqueous suspension, it was dialyzed against pure water for 48 h in order to take away the free molecules. Spectra/Por® Biotech Cellulose Ester Dialysis Membrane (MW=10,000 Da) was used.

The size of LNCs was determined by photon correlation spectroscopy method using a Malvern autosizer® 4700 (Malvern Instruments Ltd., Worcesthershure, UK) fitted by a 514 nm laser beam at a fixed angle of 90° and at T=25 °C. Only the samples of LNCs with composition: Lab, 1.028 g; Lip, 0.075 g; Sol, 0.848 g; and hydrodynamic diameter HD=50 nm were used.

By measuring the electro-kinetic properties of LNCs suspensions [6, 7], two populations of LNCs were detected: LNCs containing a small number of lipoid molecules (LNC I) having slightly negative values of the zeta potential (ZP=−5.4 mV) and LNCs with more than a critical content of lipoid molecules (LNC II) having more negative values of the zeta potential (ZP=−20 mV). Both LNCs populations were stable and remained intact in the bulk of their suspensions. A loss of mechanical stability at A/W interface leading to formation of a TG monolayer from the core of the LNCs was observed for the LNC I fraction. The lipid molecules stabilize

the LNC's structure. Thus, LNCs with smaller lipid content are expected to be more unstable at the interface in comparison to LNCs II. From experimental data and structural considerations, the percentage ratio between the two populations in the studied LNCs is evaluated as 85 % (LNCs I) to 15 % (LNCs II) [7].

Measurement at the A/W interface

The surface pressure (Π) was measured using KSV-2200 (Finland) surface balance, equipped with platinum plate and a Teflon trough with total trough area $A=475$ cm^2.

Kinetic experiments

Using Exmire microsyringe DPPC monolayers were spread at the water surface from DPPC chloroform solution ($C_{DPPC}=1$ mg×cm^{-3}) at low surface pressure $\Pi<0.2$ mN×m^{-1}. After waiting for about 10 min for solvent evaporation, the monolayers were compressed until one of desired initial surface pressures ($\Pi=1, 2, 5, 10, 15, 20,$ and 25 mN×m^{-1}) was reached. Then, the spreading of LNC dispersion containing LNC I and LNC II from a syringe at level of the water surface on preformed DPPC monolayer was done. In the cases of preformed films from Curosurf or mucus, the monolayers were obtained by spreading Curosurf® or mucus from aqueous solutions. After a period of about 30 min needed for the formation of stable surface film, the LNC dispersion was spread.

The following LNCs dispersions with concentrations of the unstable fraction LNC I estimated by means of previously described approach [7] were used: $C^*=2.5\times10^{15}, 2.5\times10^{14}$, and 2.5×10^{13} (LNC cm^{-3}). To follow the disaggregation of unstable LNCs type I, leading to rapid release of TG from the LNCs core and formation of mixed TG/DPPC, TG/Curosurf® or TG/mucus monolayers, two kinds of experiments were performed after spreading of LNCs:

(i) Recording the surface pressure (Π) change with time (t) at constant surface area (A);
(ii) Recording of the surface area change (ΔA) with time (t) at constant surface pressure (Π).

Quasiequilibrium isotherms

The isotherms $\Pi(A)$ for DPPC, Curosurf®, mucus, Labrafac® (TG), and mixed TG/DPPC monolayers were also measured and used for comparison and interpretation of kinetic data. After spreading at low surface pressure ($\Pi<0.2$ mN m^{-1}) the monolayers were compressed by means of barrier movement at sufficiently low speed ($U_b=10.8$ cm^2×min^{-1}). The quasiequilibrium isotherms $\Pi(A)$ for DPPC, Labrafac® (TG)

and mixed TG/DPPC monolayers obtained during the compression were well reproducible and practically identical at sufficiently low surface pressure with those obtained at decompression. Then, they could be used to obtain the composition TG/DPPC corresponding to the saturation of kinetic data obtained at comparable characteristic times. On the contrary, the dynamic $\Pi(A)$ isotherms for Curosurf® and mucus reveal a net hysteresis (data not shown) and cannot be considered as equilibrium ones.

All measurements were performed at room temperature ($T=23$ °C).

AFM imaging: sample preparation

The monolayers were transferred vertically on mica sheets (10×10 mm) by LB deposition where the support was immersed in the subphase before spreading either of DPPC or mucus monolayer. Next, the monolayers were compressed to $\Pi=5$ mN×m^{-1} and LNC dispersions were deposited. After a 30-min rest, the mica plate was pulled out of the subphase with a transferring rate of 5 mm×min^{-1}. The films were placed in exicator for 24 h and before imaging were blown with nitrogen gas for about 1–2 min.

NanoScope Multi Mode V AFM-system (Bruker Inc., Germany) operating in tapping mode at air with silicon cantilevers (Tap300Al-G, Innovative solutions, Bulgaria) with spring constant of $1.5\div15$ N×m^{-1} and tip radius about 20 nm. The scan rate was 1 Hz and the images were captured in height and phase modes and only flattened by Nanoscope's software (v.7.30). All samples were typically scanned in several different locations along the mica sheet and representative AFM images were chosen.

Theoretical considerations

A previously developed theoretical approach allowed us to properly analyze the behavior of LNCs spread at pure A/W interface in case of large spreading quantities and times of order of 60 min [7]. In the present paper, we expand this theoretical framework to the case of LNCs spread on preliminary formed monolayers in order to define both the rate constant k_1, the maximal degree, d_{TG}, and the effectiveness of inclusion, ε_{TG}, of TG (Labrafac®) into mixed DPPC/Labrafac® monolayer at saturation. In addition to that, we establish that the best conditions for comparison the LNCs behavior spread either at pure A/W interface or on top of a preformed monolayer correspond to small spreading LNCs quantities at times less than 1 min. In case of times less than 1 min during first rapid stage of experiment, the main contribution in $\Pi(t)$- kinetics is due to rapid disaggregation of unstable LNC I population and instantaneous Labrafac® spreading, which means that all other

processes in general kinetic scheme considered in [7] can be neglected.

The interpretation of experimental kinetic data $\Delta A(t)_{\Pi=\text{const}}$ and $\Pi(t)_{A=\text{const}}$ can be obtained on the basis of following model. A rapid disaggregation of the unstable LNCs I leads to release of confined into capsules TG molecules on the preliminary formed DPPC monolayer with rate constant k_1. During formation of a mixed TG/DPPC monolayer, the total number $n(t)$ of molecules of both species spread at whole available surface area of the trough is given by following simple expression:

$$n(t) = n_1(t) + n_2(t) = A(t)\left[\Gamma_1(t) + \Gamma_2(t)\right] \qquad (1)$$

where $n_1(t)$ and $n_2(t)$ are the number of TG and DPPC molecules, respectively in the mixed TG/DPPC monolayer formed on the whole available area $A(t) = A_0 + \Delta A(t)$; $\Gamma_1(t)$ and $\Gamma_2(t)$ are the surface concentrations of TG and DPPC molecules, respectively in unit number of molecules per unit area.

At constant surface area (A_0=const) $n_2^0 \equiv n_2(A_0) =$ const; $\Gamma_2^0 \equiv \Gamma_2(A_0)$=const for $t \geq 0$ during the spreading of TG, Eq. 1 is reduced to:

$$n(t) = n_1(t) + n_2^0 = A_0\left[\Gamma_1(t) + \Gamma_2^0\right] \qquad (2)$$

and

$$\frac{\mathrm{d}n(t)}{\mathrm{d}t} = A_0 \frac{\mathrm{d}\Gamma_1}{\mathrm{d}t}$$

Assuming that the process of disaggregation of unstable capsules type I is rate-determining, while the spreading of TG molecules confined into capsules is instantaneous, the following kinetic equation for the rate of increase of surface concentration of TG molecules in the mixed monolayer can be written as:

$$\frac{\mathrm{d}\Gamma_1}{\mathrm{d}t} = k_1(1-\theta)m_1^0 N_1 \qquad (3)$$

where k_1 is the rate constant of LNCs I disaggregation; $\theta = \frac{\Gamma_1(t) + \Gamma_2^0}{\Gamma_\infty}$ is the degree of surface coverage during formation of the mixed monolayer; $(1-\theta)$ is the part of free surface area; N_I is the number of unstable LNCs I per unit area; m_1^0 is the number of TG molecules confined in one unstable LNC of type I; $m_1^0 N_I$ is the number of TG molecules contained in all LNCs I spread at unit surface.

At the beginning of the process $\Gamma_1(t)$=0 and $\theta = \Gamma_2^0/\Gamma_\infty$; Γ_∞ is surface concentration corresponding to a close

monomolecular packing of DPPC molecules and $E_2^0 = \frac{\mathrm{d}\Pi}{\mathrm{d}\Gamma_2^0}\Gamma_2^0$ is the surface elasticity of preliminary formed DPPC monolayer. Then $\left(\frac{\mathrm{d}\Gamma_1}{\mathrm{d}\Pi}\right)_{\text{ini}} \cong \left(\frac{\mathrm{d}\Gamma_2^0}{\mathrm{d}\Pi}\right)_{\text{ini}} = \frac{\Gamma_2^0}{E_2^0}$ and finally the initial rate of increase of surface concentration of TG in mixed monolayer can be represented as:

$$\left(\frac{\mathrm{d}\Gamma_1}{\mathrm{d}t}\right)_{\text{ini}} = \left(\frac{\mathrm{d}\Gamma_1}{\mathrm{d}\Pi}\right)_{\text{ini}}\left(\frac{\mathrm{d}\Pi}{\mathrm{d}t}\right)_{\text{ini}} = \frac{\Gamma_2^0}{E_2^0}\left(\frac{\mathrm{d}\Pi}{\mathrm{d}t}\right)_{\text{ini}} \qquad (4)$$

From Eqs. 3 and 4 one obtains the following expression for the rate constant k_1:

$$k_1 = \frac{(\mathrm{d}\Pi/\mathrm{d}t)_{\text{ini}}\,\Gamma_2^0}{E_2^0(1-\theta)m_1^0 N_I} \qquad (5)$$

A maximal degree of inclusion of TG, d_{TG}, into mixed monolayer at saturation can be defined as the ratio between number of TG and DPPC species in the mixed monolayer:

$$d_{\text{TG}} = \frac{n_1^{\text{sat}}}{n_2^0} = \frac{\Gamma_1^{\text{sat}}}{\Gamma_2^0} \qquad (6)$$

The corresponding effectiveness of inclusion, ε_{TG}, is given as the ratio between the numbers of TG molecules included in the surface film at saturation as a result of LNC I disaggregation and those contained in all spread LNCs:

$$\varepsilon_{\text{TG}} = \frac{n_1^{\text{sat}}}{m_1^0 N_I A} = \frac{\Gamma_1^{\text{sat}}}{m_1^0 N_I} \qquad (7)$$

When all TG molecules contained in all spread LNCs are included in the surface monolayer, then ε_{TG}=1.

The values of Γ_1^{sat} and then of d_{TG} and ε_{TG} can be estimated in two ways. The first one considers the change of surface pressure from $\Pi_{0\ \text{DPPC}}$ to $\Pi_{\text{sat TG/DPPC}}$ which is then compared with independently measured isotherm network for obtaining the composition of mixed TG/DPPC monolayer, x_{TG}, resp. Γ_1^{sat} corresponding to the saturation.

In the second one, after integrating Eq. 4 from t=0 to t_{sat} and using the experimental values for E_2^0, we can also estimate the values for Γ_1^{sat} as follows:

$$\Gamma_1^{\text{sat}} \cong \int_0^{t\text{sat}} \frac{\Gamma_2^0}{E_2^0}\left(\frac{\mathrm{d}\Pi}{\mathrm{d}t}\right)_{\text{ini}} \mathrm{d}t \qquad (8)$$

In the case when LNCs spread on pure A/W interface form a pure TG monolayer (Γ_2=0), Γ_1^{sat} can be determined by

comparison with the isotherm $\Pi(A=1/\Gamma)$ for pure TG monolayer

The rate constant k_1 in this case of formation of pure TG monolayer can be estimated from Eq. 3 as follows:

$$k_1 = \frac{\left(\Gamma_{TG}^{sat}/t_{sat}\right)}{\left(1-\theta_{TG}^{sat}\right)m_1^0 N_1} \tag{9}$$

At constant surface pressure (Π=const)

If assuming an ideal behavior of the formed mixed TG/DPPC monolayer, we can consider the initial surface area A_0 as covered by DPPC molecules and the observed surface area change (ΔA) covered only by TG molecules with constant surface densities Γ_1^0 and Γ_2^0, respectively. Then, the Eq. 1 is reduced to:

$$n(t) = n_1(t) + n_2^0 = \Delta A(t)\Gamma_1^0 + A_0\Gamma_2^0 \tag{10}$$

From Eq. 10, we can determine also the values for maximal degree of inclusion d_{TG} of TG in DPPC monolayer as follows:

$$d_{TG} = \frac{\Delta A_{sat}\Gamma_1^0}{A_0\,\Gamma_2^0} \tag{11}$$

and the corresponding effectiveness of inclusion ε_{TG} as:

$$\varepsilon_{TG} = \frac{\Delta A_{sat}\Gamma_1^0}{m_1^0 N_I A} \tag{12}$$

Finally, we have to underline that the theoretical analysis of experimental data assumes that when an aqueous dispersion of LNC has been spread on the top of existing monolayer of either DPPC, Curosurf®, or mucus the spreading procedure is quantitative, i.e., there is no loss of material in bulk phase during the spreading process.

Results and discussion

Isotherms of the studied monolayers

The quasiequilibrium isotherms $\Pi(A=1/\Gamma)$ for various compositions X_{Lab} of model mixed Lab/DPPC monolayers were presented in Fig. 1a. They were used to obtain the values for Γ_{Lab} at saturation after comparison with the $\Pi(t)$ kinetic data.

The Labrafac® is a mixture of C:8 and C:10 TG and curve 7 at Fig. 1a corresponds to $\Pi(A)$ isotherm of pure Labrafac® monolayer in liquid-expanded (LE) state with collapse at $\Pi\approx22$ mN×m^{-1} a value which is in the same order of
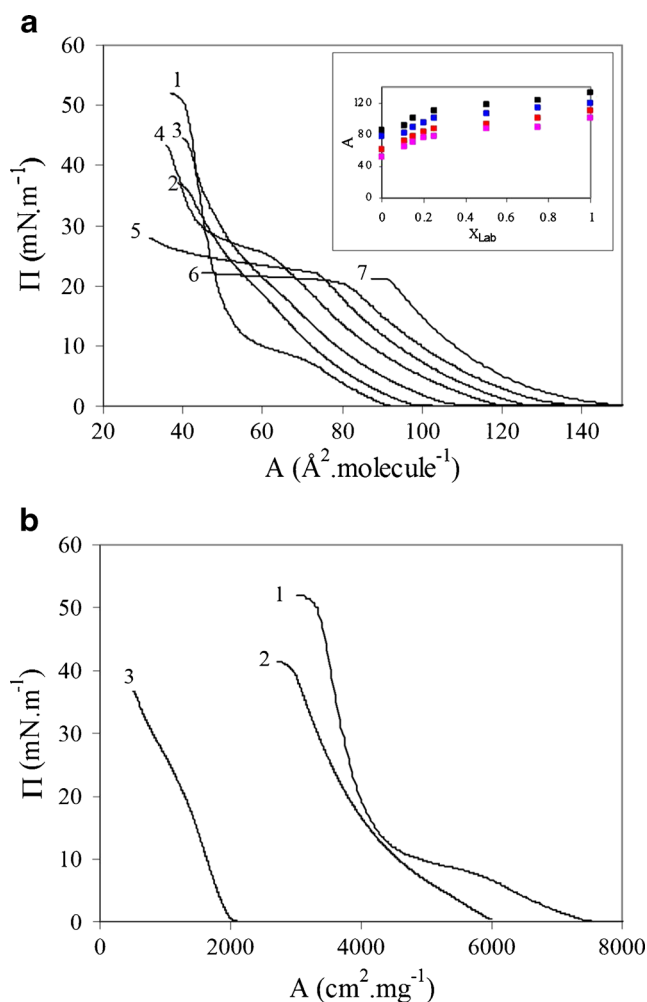
Fig. 1 **a** Surface pressure (Π)/mean area $\left(\overline{A}\right)$ per molecule isotherms of mixed Labrafac®/DPPC monolayers: *curve 1*, pure DPPC; *curve 7*, pure Labrafac®; *curves 2–6*, mixed Lab/DPPC monolayers with different molecular ratio X_{Lab}: *2*, X_{Lab}=0.11; *3*, X_{Lab}=0.15; *4*, X_{Lab}=0.25; *5*, X_{Lab}=0.50; *6*, X_{Lab}=0.75 (*inset*, $\overline{A}$ versus X_{Lab} for a mixed Labrafac®/DPPC monolayers at Π=2 mN×m^{-1} (*black square*); 5 mN×m^{-1} (*blue square*); 10 mN×m^{-1} (*red square*); 15 mN×m^{-1} (*pink square*); **b** $\Pi(A)$ isotherms of DPPC, Curosurf®, and mucus expressed in cm^2×mg^{-1}: *curve 1*, DPPC; *curve 2*, Curosurf®; and *curve 3*, mucus)

magnitude as the collapse surface pressure of both TG components of Labrafac®. Curve 1 in Fig. 1a corresponding to $\Pi(A)$ isotherm of pure a DPPC monolayer demonstrates the well-known liquid-expanded/liquid-condensed (LE/LC) phase transition at Π=6 mN×m^{-1}. The compositions with increasing DPPC quantities (starting at Fig. 1a from curve 6 with X_{DPPC}=0.25 to curve 2 with X_{DPPC}=0.89) show that LE/LC phase transition was influenced by the presence of Labrafac®. The inset in Fig. 1a representing the mean molecular area $\overline{A}$ as a function of molar ratio X_{Lab} indicates miscibility with a slightly practically negligible positive deviation from additivity.

The peculiar observation in Fig. 1a concerning the shift of curves 2, 3, and 4 to molecular areas smaller than that of pure

DPPC does not really make sense. However, this result can be explained with the presence of soluble components in Labrafac®, which are squeezed out from the monolayer at larger surface pressures. Such effect is not taken into account in the calculation of mean area $\overline{A}$ of mixed Lab/DPPC monolayers.

The $\Pi(A)$ isotherms of the three studied preformed monolayers—DPPC, Curosurf®, and mucus, are also presented in Fig. 1b. Considering the complex composition of Curosurf® and mucus, the areas in Fig. 1b were expressed in square centimeters per milligram. For comparison, the isotherm of DPPC monolayer in Fig. 1b was also transposed in the same units.

We have to note that in case of monolayer formed from natural mixture such as mucus fluid, obviously it is difficult to accurately determine whether this material will retain its structure and properties after spreading at A/W interface. Nevertheless, it may be assumed that the network formed by negatively charged mucin fibers could preserve and maintain an interfacial organization not much different from that, which exists in the mucus layer covering luminal surface of gastrointestinal tract.

Spreading of different LNCs quantities at pure A/W interface

The $\Pi(t)_{A=\text{const}}$ results obtained after spreading of different LNCs quantities N_I (column 1 of Table 1) on pure A/W interface are presented in Fig. 2. The observed large jump between curves 3 and 4 at Fig. 2 is due to the large difference of surface compressibility modulus $C_s^{-1} \equiv E$ ($E_{\text{Lab}(3)}=35$ mN×m^{-1}; $E_{\text{Lab}(4)}=71$ mN×m^{-1}). We have to note that the surface pressure at saturation (Π_{sat}) corresponding to close packing of Labrafac® monolayer cannot be reached within the experimental framework of spreading LNC quantities N_I (i.e., from 0.3×10^{10} to 3.2×10^{10} LNC cm^{-2}). For comparison, in the previous paper [7], the maximal saturation in Labrafac® monolayer at $\Pi=22$ mN×m^{-1} corresponded to collapse surface pressure, which has been obtained for $N_I=1.2 \times 10^{11}$ LNC×cm^{-2}.
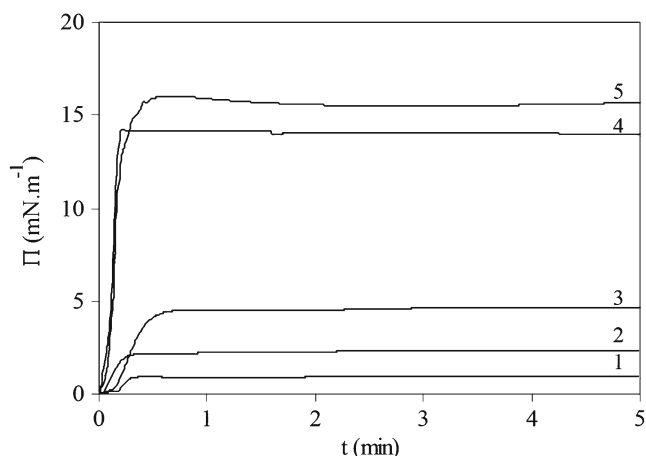

Fig. 2 Evolution of surface pressure (Π) with time (t) at $A=$constant after spreading different LNCs quantities N_I (in LNC×cm^{-2}) on pure A/W interface: *curve 1*, $N_I=0.3.10^{10}$; *curve 2*, $N_I=0.5 \times 10^{10}$; *curve 3*, $N_I=0.8 \times 10^{10}$; *curve 4*, $N_I=1.6 \times 10^{10}$; *curve 5*, $N_I=3.2 \times 10^{10}$

The slight delay of surface pressure increase in curves 1 and 3 and the slight difference in the course of kinetic curve 4 (Fig. 2) recorded in the first 10 s has no physical meaning because this time is comparable with the time of LNCs spreading procedure.

By comparing the values of surface pressure at saturation Π_{sat} (column 3, Table 1) with $\Pi(A)$ isotherm for Labrafac® monolayer (Fig. 1a, curve 7), the values for $\Gamma_{\text{TG}}^{\text{sat}}$ (column 4, Table 1) and according to Eq. 7 determined the values of effectiveness of inclusion ε_{TG} (column 7, Table 1). Using the experimental data for $\Gamma_{\text{TG}}^{\text{sat}}/t_{\text{sat}}$, for $\theta_{\text{TG}}^{\text{sat}}=\Gamma_{\text{TG}}^{\text{sat}}/\Gamma_\infty$ from $\Pi(A)$ isotherm of Labrafac® and Eq. 9 applied for the case of LNCs spreading on pure A/W interface, the values of the rate constant k_1 of LNCs disaggregation (column 8, Table 1) are also estimated.

At smallest LNCs spreading quantity $N_I=0.3 \times 10^{10}$ LNC×cm^{-2}, the monolayer at saturation is formed from all TG molecules contained in all spread LNCs type I and the effectiveness of disaggregation of the LNCs is 100 % ($\varepsilon_{\text{TG}}=1$). When the LNCs spreading quantity N_I increases, then the effectiveness, ε_{TG}, at the saturation

Table 1 Spreading of different LNCs quantities on pure A/W interface

1 N_I $\left(\dfrac{\text{LNC}}{\text{cm}^2}\right)$	2 $m_1^0 N_I$ $\left(\dfrac{\text{molTG}}{\text{cm}^2}\right)$	3 Π_{sat} $\left(\dfrac{\text{mN}}{\text{m}}\right)$	4 $\Gamma_{\text{TG}}^{\text{sat}}$ $\left(\dfrac{\text{molTG}}{\text{cm}^2}\right)$	5 $\theta_{\text{TG}}^{\text{sat}}$	6 $\Delta\Gamma_{\text{TG}}/\Delta t$ $\left(\dfrac{\text{molTG}}{\text{cm}^2\ \text{min}}\right)$	7 $\varepsilon_{\text{TG}}=\dfrac{\Gamma_{\text{TG}}^{\text{sat}}}{m_1^0 N_I}$	8 k_1 (min^{-1})
0.3×10^{10}	0.69×10^{14}	0.93	0.68×10^{14}	0.60	1.5×10^{14}	1.00	5.8
0.5×10^{10}	1.15×10^{14}	2.20	0.77×10^{14}	0.70	2.2×10^{14}	0.67	6.8
0.8×10^{10}	1.85×10^{14}	4.60	0.83×10^{14}	0.83	2.1×10^{14}	0.45	6.7
1.6×10^{10}	3.68×10^{14}	14.0	1.00×10^{14}	0.91	5.0×10^{14}	0.27	15.1
3.2×10^{10}	7.36×10^{14}	15.9	1.04×10^{14}	0.95	5.2×10^{14}	0.14	14.1

decreases. This effect could be related either to partial stabilization of the LNCs given their interaction with the already formed TG monolayer at the latter stage of spreading or/and to the fact that part of the free surface $(1-\theta)$ diminishes from 0.40 to 0.05.

The estimated values of the rate of LNCs disaggregation k_1 are ranging between 5 and 15 min^{-1}.

To understand better the loss of LNCs mechanical stability at pure A/W interface or covered by preformed monolayer models of membranes, the small spreading LNCs quantities showing $\varepsilon_{TG}=1$ at pure A/W interface were studied and compared. One of the reasons to study the behavior of LNCs spread at small quantities was the observation that at smallest LNCs spreading quantities, the monolayer at saturation is formed from all Labrafac® molecules contained in all spread LNCs type I, i.e., there is no loss of material during the spreading procedure of LNC at A/W interface.

Spreading of small LNCs quantities on preliminary formed DPPC monolayer

The Π $(t)_{A=const}$ results obtained after spreading of small LNCs quantities N_I from 0.41 to 0.84×10^{10} and from 0.05 to 0.08×10^{10} LNC cm^{-2}, corresponding to ratio 1:1, respectively 1:10 between the TG molecules confined in all LNCs and DPPC molecules in the previously spread DPPC monolayer at various surface pressures $\Pi=1, 2, 5, 10, 15, 20,$ and 25 mN$\times$m^{-1} are presented in Fig. 3a. The observed large jump between curves 3 and 4 seems to take place at the same surface pressure where DPPC undergoes a phase transition. The heterogeneous structure of monolayer probably plays a decisive role in interfacial mechanical stability of LNCs as it would be seen and discussed later from AFM data, where LNCs are attached preferably at the boundary between the two coexisting DPPC phases. In addition, as observed in Fig. 2, the jump may also be related to differences of the surface compressibility modulus $C_s^{-1}\equiv E$ ($E_{DPPC(3)}=39$ mN m^{-1}; $E_{DPPC(4)}=68$ mN m^{-1}).

The values for Γ_{TG}^{sat} are obtained either by comparison with the mixed TG/DPPC monolayer $\Pi(A)$ isotherms presented in Fig. 1 or from experimental values for the surface elasticity E_{DPPC} and Eq. 8. The values for d_{TG}, ε_{TG}, and k_1 corresponding to the same spreading LNCs quantities obtained from both procedures are practically identical. The summarized results for d_{TG}, ε_{TG}, and k_1 obtained from experimental data $\Pi(t)_{A=const}$ using both approaches are presented in Table 2.

The $\Delta A(t)_{\Pi=const}$ results obtained after spreading of LNCs quantities $N_I=0.55\div0.84\times10^{10}$ and 0.05 to 0.08×10^{10} LNC cm^{-2} are presented at Fig. 3b. The interpretation of $\Delta A(t)$ at $\Pi_0=const$ is based on Eqs. 10, 11, and 12. The obtained values for d_{TG} and ε_{TG} differ slightly from those obtained by two previous ways of calculation at $A_0=const$
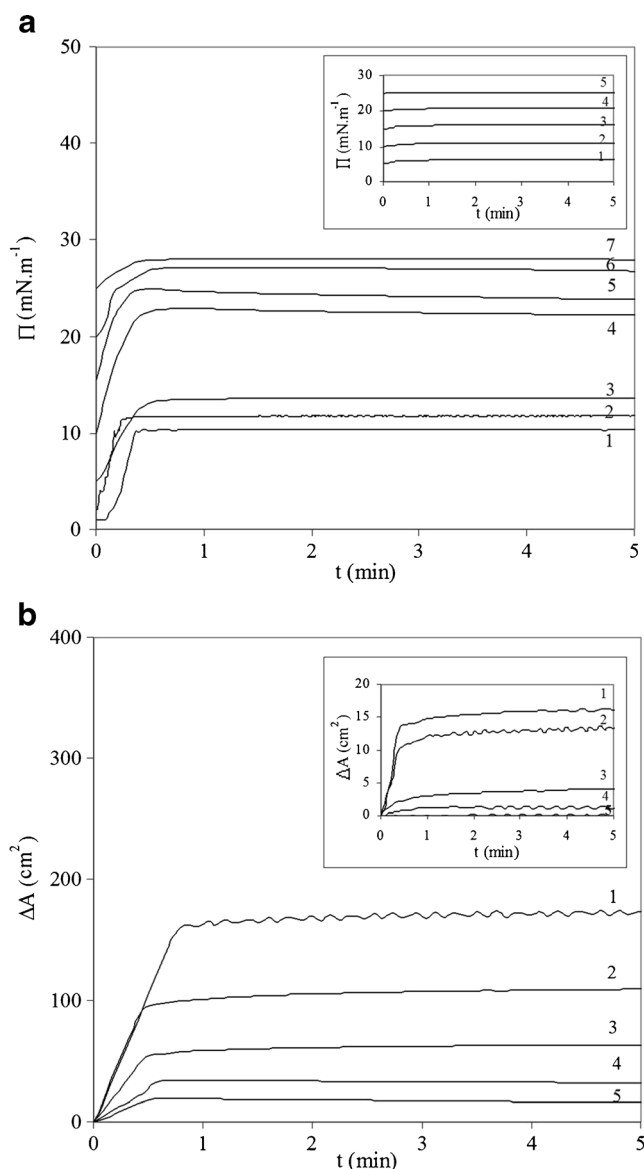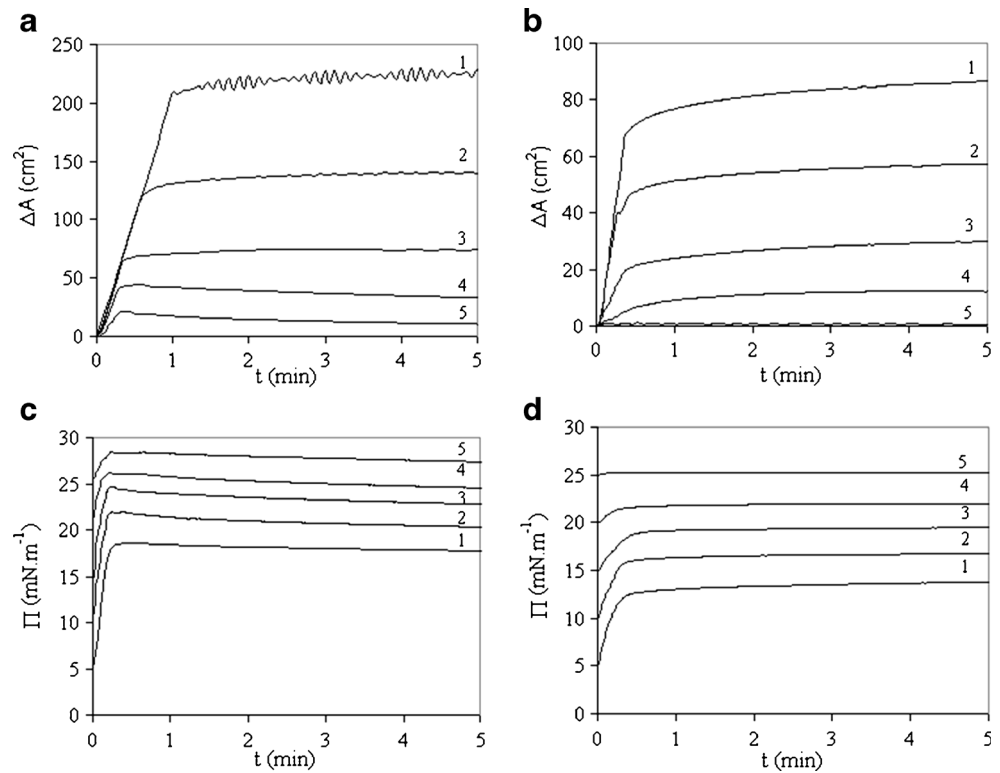

Fig. 3 **a** $\Pi(t)_{A=const}$ after spreading of LNCs on preliminary formed DPPC monolayer; molecular ratio Lab/DPPC (1:1) at various surface pressure: *curve 1*, $\Pi=1$ mN$\times$m^{-1}; *curve 2*, $\Pi=2$ mN$\times$m^{-1}; *curve 3*, $\Pi=5$ mN$\times$m^{-1}; *curve 4*, $\Pi=10$ mN$\times$m^{-1}; *curve 5*, $\Pi=15$ mN$\times$m^{-1}; *curve 6*, $\pi=20$ mN$\times$m^{-1}; and *curve 7*, $\Pi=25$ mN$\times$m^{-1} (*inset* corresponds to molecular ratio Lab/DPPC 1:10 at surface pressures $\Pi=5, 10, 15, 20,$ and 25 mN$\times$m^{-1}); **b** $\Delta A(t)_{\Pi=const}$ after spreading of LNCs on preliminary formed DPPC monolayer; molecular ratio Lab/DPPC (1:1) at various surface pressure: *curve 1*, $\Pi=5$ mN$\times$m^{-1}; *curve 2*, $\Pi=10$ mN$\times$m^{-1}; *curve 3*, $\Pi=15$ mN$\times$m^{-1}; *curve 4* $\Pi=20$ mN$\times$m^{-1}; and *curve 5*, $\Pi=25$ mN$\times$m^{-1} (*inset* corresponds of molecular ratio Lab/DPPC 1:10 at the same surface pressures)

(data not shown). Nevertheless, the same dependence on the LNCs spread quantities is observed. As far as the observed small differences are concerned it is important to note that the process of LNCs destabilization and disaggregation occurs in better defined thermodynamic conditions at $\Pi_0=const$ than at $A_0=const$.

Fig. 4 $\Delta A(t)_{\Pi=\text{const}}$ (**a**) and $\Pi(t)_{A=\text{const}}$ (**c**) after spreading of LNCs on preformed Curosurf® monolayer at various surface pressures: *curve 1*, $\Pi=5$ mN× m^{-1}; *curve 2*, $\Pi=10$ mN×m^{-1}; *curve 3*, $\Pi=15$ mN×m^{-1}; *curve 4*, $\Pi=20$ mN×m^{-1}; and *curve 5*, $\Pi=25$ mN×m^{-1}; $\Delta A(t)_{\Pi=\text{const}}$ (**b**) and $\Pi(t)_{A=\text{const}}$ (**d**) after spreading of LNCs on preformed mucus monolayer at the same surface pressures (Π)

Comparison between the obtained results for LNCs spread at pure A/W interface and on a DPPC monolayer

The comparison between the obtained results for LNCs spread at pure A/W interface (Table 1) and on the top of preliminary formed DPPC monolayer (Table 2) suggests that the interaction between LNCs and DPPC monolayer is responsible for a partial LNCs stabilization. For example, at approximately the same $N_I=0.3\div0.41\times10^{10}$ LNC×cm^{-2}, $\Pi=0.93\div1.0$ mN× m^{-1}, and $\theta=0.50\div0.60$, the effectiveness of LNC spreading ε_{TG} given as the ratio between the numbers of TG molecules included in the surface film at saturation as a result of LNC I disaggregation and those contained in all spread LNCs and rate constant of LNC disaggregation k_1 are $\varepsilon_{\text{TG}}=1$ and $k_1=5.8$ min^{-1} on pure A/W interface while at preformed DPPC monolayer the effectiveness and the rate of disaggregation

Table 2 Spreading of small LNCs quantities at $A_0=$const on preformed DPPC monolayers

1 Π_{DPPC}^0 $\left(\dfrac{\text{mN}}{\text{m}}\right)$	2 N_I $\left(\dfrac{\text{LNC}}{\text{cm}^2}\right)$	3 $\theta_{\text{DPPC}}=\dfrac{\Gamma^0}{\Gamma_\infty}$	4 $d_{\text{TG}}=\dfrac{\Gamma_{\text{TG}}^{\text{sat}}}{\Gamma_{\text{DPPC}}^0}$	5 $\varepsilon_{\text{TG}}=\dfrac{\Gamma_{\text{TG}}^{\text{sat}}}{m_1^0 N_I}$	6 k_1 (min^{-1})
1	0.41×10^{10}	0.50	0.510	0.51	2.7
2	0.44×10^{10}	0.52	0.430	0.43	2.9
5	0.05×10^{10}	0.65	0.030	0.32	1.9
	0.55×10^{10}	0.65	0.280	0.27	1.8
10	0.08×10^{10}	0.78	0.020	0.18	1.2
	0.76×10^{10}	0.78	0.230	0.17	2.3
15	0.08×10^{10}	0.83	0.010	0.11	1.1
	0.76×10^{10}	0.83	0.120	0.12	2.4
20	0.08×10^{10}	0,88	0.005	0.05	0.9
	0.84×10^{10}	0.88	0.090	0.09	1.9
25	0.08×10^{10}	0.91	0.001	0.01	0.2
	0.75×10^{10}	0.91	0.030	0.03	1.0

are smaller $\varepsilon_{TG}=0.51$ and $k_1=2.7$ min^{-1}. The same effect—larger ε_{TG} and k_1 for pure A/W interface than for DPPC monolayer is observed also for studied quantities $N_I=0.5 \div 0.55 \times 10^{10}$ LNC×cm^{-2} ($\varepsilon_{TG}=0.67$ and $k_1=6.8$ min^{-1} versus $\varepsilon_{TG}=0.27$ and $k_1=1.8$ min^{-1}) and $N_I=0.8 \div 0.76 \times 10^{10}$ LNC×cm^{-2} ($\varepsilon_{TG}=0.45$ and $k_1=6.7$ min^{-1} versus $\varepsilon_{TG}=0.17$ and $k_1=2.3$ min^{-1}). Thus, the comparison suggests that the observed difference in the effectiveness of LNC spreading, ε_{TG}, and rate of disaggregation, k_1, for LNCs spread at the pure A/W interface and on preformed DPPC monolayer is due to the LNC partial stabilization and not to the lack of free surface area $(1-\theta)$.

As it was shown in "Spreading of different LNCs quantities at pure air-water interface" when LNCs spreading quantity, N_I, increase the observed decrease of the effectiveness, ε_{TG}, could be in principle related either to the LNCs partial stabilization or to the lack of free surface area $(1-\theta)$. The idea that a partial LNCs stabilization occurs as a result of the interaction with the A/W surface covered by DPPC molecules is also confirmed by the fact that at the same part of free surface area $(1-\theta)$, the same effectiveness ε_{TG} and rate of disaggregation k_1 are obtained with 10-fold larger LNCs spread quantities N_I and degree of inclusion d_{TG}. For example, at the same $\Pi=5$ mN×m^{-1} (Table 2) and the same part of free surface area $(1-\theta)=0.35$ for $N_I=0.05 \times 10^{10}$ LNC×cm^{-2} and for $N_I=0.55 \times 10^{10}$ LNC×cm^{-2}, the obtained values $d_{TG}=0.030$, $\varepsilon_{TG}=0.32$, $k_1=1.9$ min^{-1} and $d_{TG}=0.280$, $\varepsilon_{TG}=0.27$, $k_1=1.8$ min^{-1} respectively are practically the same.

Spreading of small LNCs quantities on preliminary formed Curosurf® and mucus monolayers

The $\Delta A(t)_{\Pi=const}$ and $\Pi(t)_{A=const}$ results obtained after spreading of 0.028 mg TG (1.43×10^{12} LNC) on the whole monolayer area covered with 0.071 mg Curosurf® are presented in Fig. 4a, c. The interpretation of experimental data is as described above and the obtained results for d_{TG}, ε_{TG}, and k_1 are presented in Table 3. The ratio between TG and Curosurf® is expressed as mg per mg because of the complex composition of Curosurf®. To compare d_{TG} and ε_{TG}, the units for DPPC monolayer were also transposed in mg instead of molecules. The obtained values for effectiveness ε_{TG}, of LNCs disaggregation on Curosurf® monolayer were close to those on DPPC monolayer. This finding seems logical because DPPC is the main component of Curosurf®.

The results $\Delta A(t)_{\Pi=const}$ and $\Pi(t)_{A=const}$ obtained after spreading of 0.011 mg TG (1.43×10^{12} LNC) on the whole monolayer area covered with 0.17 mg mucus are presented in Fig. 4b, d. The values for d_{TG}, ε_{TG}, and k_1 obtained by means of the above-described approach are summarized and presented also in Table 3.

At the same lateral surface pressure, the effectiveness ε_{TG} of LNCs disaggregation on mucus monolayer decreases and mechanical stability increases in comparison with those on DPPC monolayer.

As far as the molecular nature of LNCs–model membrane monolayers interaction is concerned, the obtained results
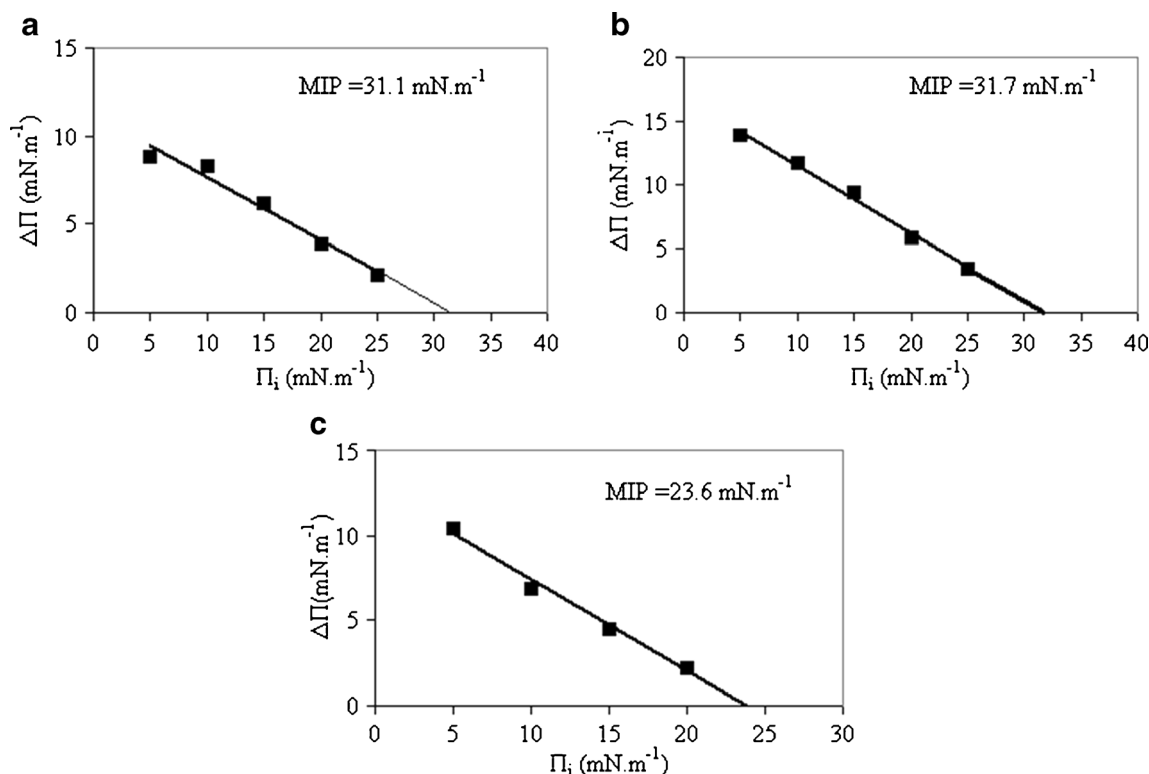

Fig. 5 Determination of MIP of TG from disaggregated LNCs into DPPC (a), Curosurf® (b), and mucus (c) monolayers

about LNCs mechanical stability viewed at phenomenological level by ε_{TG} seem to be in accordance with the common understanding about the role of electrostatic "particle–monolayer" interactions [24]. The interaction between LNCs and monolayer model membrane determining the mechanical stability (or instability) is a result of superposition of various electrostatic and hydrophobic interactions. The observation that the LNCs are more stable when spread at mucus rather than on top of DPPC or Curosurf® monolayer could be explained by the electrostatic interaction between them. Actually, the particle shell of LNCs is slightly negatively charged. From measurements of electro-kinetic properties of LNC suspensions [6, 7], the values for zeta potential ZP=−5.4 mV for LNC I fraction without or containing only small number of lipoid molecules and respectively ZP=−20 mV for the LNC II fraction with more than a critical content of lipoid molecules were obtained. The LNCs have negative zeta potential [25] very close to the ZP of other carriers containing PEG such as liposomes because the LNCs shells contain hydrophilic surfactants with PEG chains [26]. The phosphate groups of phospholipid molecules presented in larger quantity in LNC II fraction should increase the electro-negativity if we assume that they can deliver these charges at the external part of shell. On the other side, the mucus is composed of negatively charged mucin fibers [27]. These negative charges in the plane of the monolayer could be partly responsible for the mucin-LNC electrostatic repulsion leading to LNCs stabilization.

In opposition to all that, the monolayers of DPPC as well as Curosurf®, where the main component is DPPC, are composed of neutral molecules. Thus, no electrostatic repulsion between LNCs and either of DPPC or Curosurf® monolayers are expected.

Maximal insertion pressure of the studied systems

The degree of inclusion strongly depends on surface pressure of the preliminary spread monolayer and it is usually characterized by the so-called maximal insertion pressure (MIP) [28].

From the experimental $\Pi(t)$ data presented in Figs. 3a and Fig. 4c, d represented in the scale increase of surface pressure $\Delta\Pi$ as function of the initial surface pressure Π_i Fig. 5 the following values for MIP: MIP=31.1 and 31.7 mN×m^{-1} were obtained for DPPC and Curosurf® monolayers, respectively, and MIP=23.6 mN×m^{-1} for mucus monolayer. The larger values of MIP imply that the penetration of TG into DPPC and Curosurf® monolayer is easier than into the mucus monolayer.

AFM imaging

It is well-established that DPPC monolayer undergoes a first-order phase transition from liquid-expanded (LE) phase to liquid-condensed (LC) phase, as a result of process driven by a competition between line tension and electrostatic forces [29]. The LE/LC transition in monolayers has been structurally well characterized on micrometer scale level by fluorescence and Brewster angle microscopies [30]. It was also shown that the coexisting lateral structure of phospholipid monolayers can be preserved after their transfer via LB technique on solid mica supports for AFM imaging [31]. Following the same protocol as in [31], we imaged the state of preformed DPPC and mucus monolayers in presence of LNCs.

At Fig. 6a are presented AFM image showing the topography of DPPC/LNCs film with embedded into DPPC monolayer two LNCs. Scanning over different areas of the films showed that only few LNCs entrenched in DPPC monolayer were identified. The LE/LC phase separation within DPPC monolayer is confirmed by high resolution topography image shown as an inset in Fig. 6a where the darker areas represent LE phase and brighter LC phase. It follows from the measured height difference between the coexisting phases which is $\Delta h \approx 0.6$ nm. It is in agreement with the length difference between DPPC carbon chains when the monolayer is in LE and LC phases. Figure 6a also demonstrates that two-phase

Table 3 Spreading of small LNCs quantities at Π_0=const on preformed DPPC, Curosurf®, and Mucus monolayers: Spread on the whole surface area quantities: DPPC, 0.04 mg; TG, 0.028 mg ($m_1^0 NA_0 = 1.43 \times 10^{12}$ LNC); Curosurf®, 0.071 mg; TG, 0.011 mg ($m_1^0 NA_0 = 0.6 \cdot 10^{12}$ LNC); mucus, 0.17 mg; TG, 0.011 mg; Γ_2^0 is the surface density at initial surface area A_0 for DPPC, Curosurf® and mucus, respectively

Π^0 (mN m^{-1})	$d_{TG} = \frac{\Gamma_{TG}^{sat}}{\Gamma_2^0}$	$\varepsilon_{TG} = \frac{\Gamma_{TG}^{sat}}{m_1^0 N_I}$	k_1 (min^{-1})
DPPC			
5	0.28	0.40	1.8
10	0.19	0.26	2.3
15	0.12	0.18	2.4
20	0.08	0.11	1.9
25	0.04	0.05	1.0
Curosurf®			
5	0.20	0.49	6.8
10	0.13	0.33	7.1
15	0.08	0.21	4.6
20	0.06	0.15	3.5
25	0.03	0.07	1.9
Mucus			
5	0.03	0.19	6.9
10	0.02	0.14	4.9
15	0.01	0.07	3.8
20	0.01	0.04	5.5
25	0.00	0.01	0.0

lipid organization favors the attachment of LNCs at the boundary between LE and LC phases. A similar preference of lipolytic enzyme PhospholipaseA$_2$ (PLA$_2$) to accumulate along the LC/LE domain boundaries is reported [32]. The measured height of LNCs about 18±2.0 nm indicates for partially disintegration of LNCs which initial diameter before spreading on A/W interface was about 50 nm.

At Fig. 6b are presented AFM images and cross-section graphs of pure mucus monolayer transferred on mica support at 5 mN×m^{-1} (left image) and preformed mucus monolayer with LNCs (right image) where the differences in their

Fig. 6 **a** AFM topography images of LB films transferred from DPPC monolayer compressed to Π=5 mN×m^{-1} followed by deposition of LNC dispersion (*inset* is area zoom with z=10 nm). Beneath, cross-section of LNCs, embedded into DPPC; **b** AFM topography images of LB films of pure mucus monolayer (*left image*) and AFM image of LB film from preformed mucus monolayer with LNCs (*right image*). The *insets* are particular cross-sections

morphologies are easily distinguishable. The morphology of pure mucus films show only an existence of embedded proteins as a part of the mucus content, which have sizes of about 5 nm, a typical value for globular proteins or enzymes [33, 34]. The AFM image of mixed mucus/LNCs LB films shows an abundance of 3D-structures with sizes of about 3÷5 nm which are grafted in mucus layer. There is also a population of 3D-structures which could be LNCs embedded in the mucus layer because of their much bigger size (10÷15 nm) close to the size of LNCs imaged in DPPC/LNCs system. The differences in the morphologies between pure mucus and mucus/LNCs films are also confirmed from the roughness analysis which shows the estimated mean roughness of 0.179 nm for mucus and about 0.478 nm for mucus/LNCs.
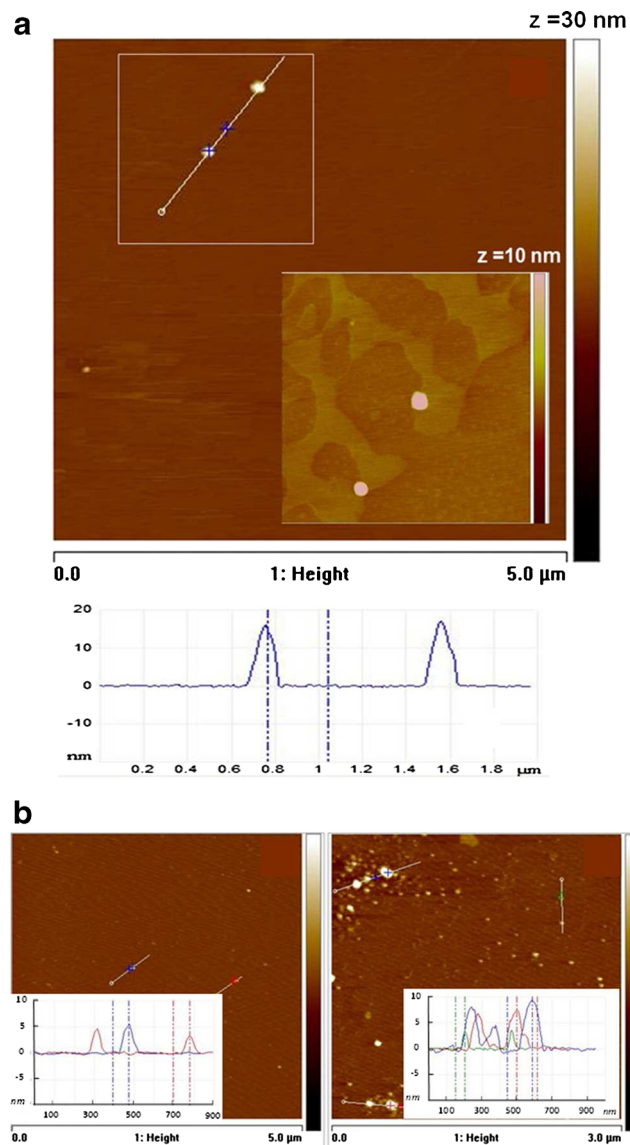
Conclusions

A loss of mechanical stability of LNCs spread at pure A/W interface or at preformed model membrane monolayers is observed. The LNCs undergo a partial destabilization, disaggregation, and formation of pure or mixed surface films. The comparison between the effectiveness of spreading (ε_{TG}) and the rate of LNC disaggregation (k_1) at pure A/W interface and at preformed DPPC monolayer indicates a partial LNCs stabilization due to LNCs-DPPC interaction. The comparison between effectiveness of inclusion of TG (ε_{TG}) into model membrane monolayers of DPPC, Curosurf®, and mucus shows that the LNCs spread on mucus surface layer are more stable and interact stronger with the monolayer than if they are spread on DPPC and Curosurf® monolayers. These findings are in accordance with AFM images showing more 3D structures grafted in mucus layer than in DPPC monolayer. As far as the molecular nature of LNCs—model membrane monolayer interactions are concerned, additional approaches and techniques are needed to develop a conclusive molecular model of the behavior of LNCs spread on various model membrane systems.

From physiological point of view, we hope that such approach could provide some new insights and suggestions about the behavior of LNCs at membranes interfaces. The choice of Curosurf® and mucus monolayers as membrane models was mainly provoked by the attempts which are now in progress various liposoluble drugs to be administrated via LNCs towards alveolar surface and luminal surface of gastrointestinal tract thus proving their effectiveness as drug delivery systems. Obviously, it is a difficult task to bridge the existing gap between monolayer model system and LNCs behavior in physiological medium. Although, in the future we intend to find a way to correlate the results obtained from the developed 2D model of LNCs–membrane interaction with the results from 3D drug delivery model systems.

References

1. Heurtault B, Saulnier P, Pech B, Proust J, Benoit JP (2002) A novel phase inversion-based process for the preparation of lipid nanocarriers. Pharm Res 19:875–880
2. Heurtault B, Saulnier P, Pech B, Venier-Julienne MC, Proust J, Phan-Tan Luu R, Benoit JP (2003) The influence of lipid nanocapsule composition on their size distribution. Eur J Pharm Sci 18:55–61
3. Anton N, Saulnier P, Béduneau A, Benoit JP (2007) Salting-out effect induced by temperature cycling on a water/nonionic surfactant/oil system. J Phys Chem B 111:3651–3657
4. Hirsjärvi S, Dufort S, Bastiat G, Saulnier P, Passirani C, Coll JL (2013) Surface modification of lipid nanocapsules with polysaccharides: from physicochemical characteristics to in vivo aspects. Acta Biomater 9:6686–6693
5. Malzert-Fréon A, Saint-Lorant G, Hennequin D, Gauduchon P, Poulain L, Rault S (2010) Influence of the introduction of a solubility enhancer on the formulation of lipidic nanoparticles with improved drug loading rates. Eur J Pharm Biopharm 75:117–127
6. Perrier T, Saulnier P, Fouchet F, Lautram N, Benoit JP (2010) Post-insertion into Lipid NanoCapsules (LNCs): from experimental aspects to mechanisms. Int J Pharm 396:204–209
7. Minkov I, Tz I, Panaiotov I, Proust J, Saulnier P (2005) Reorganisation of lipid nanocapsules at air-water interface: 1. Kinetics of surface film formation. Colloids Surf B: Biointerfaces 45:14–23
8. Minkov I, Tz I, Panaiotov I, Proust J, Saulnier P (2005) Reorganisation of lipid nanocapsules at air-water interface: 2. Properties of the formed surface film. Colloids Surf B: Biointerfaces 44:197–203
9. Minkov I, Tz I, Panaiotov I, Proust J, Verger R (2005) Reorganisation of lipid nanocapsules at air–water interface: 3. Action of hydrolytic enzymes HLL and PLA$_2$. Colloids Surf B: Biointerfaces 45:32–41
10. Minkov I, TZ I, Panaiotov I, Proust J, Saulnier P (2009) Kinetics of reorganization of lipid nanocapsules at air–water interface. Ann Univ Sofia FacChem 101:45–57
11. Zhao L, Feng S (2005) Effects of lipid chain unsaturation and headgroup type on molecular interactions between paclitaxel and phospholipid within model biomembrane. J Colloid Interface Sci 285:326–335
12. Villallonga F (1968) Surface chemistry of l-α-dipalmitoyl lecithin at the air-water interface. BBA 163:290–300
13. Phillips MC, Chapman D (1968) Monolayer characteristics of saturated 1,2-diacyl phosphatidylcholines (lecithins) and phosphatidylethanolamines at the air-water interface. BBA 163:301–313
14. Phillips MC (1972) Progress in Surface and Membrane Science, Academic Press, New York, 5:139–221
15. Taneva S, Panaiotov I, Ter-Minassian Saraga L (1984) Effect of surface pressure on mixed dipalmitoyllecithin-serum albumin monolayer composition. Coll and Surf 10:101–111
16. Chimote G, Banerjee R (2008) Evaluation of antitubercular drug insertion into preformed dipalmitoylphosphatidylcholine monolayers. Colloids Surf B: Biointerfaces 62:258–264
17. Notter RH, Tabak SA, Mavis RD (1980) Surface properties of binary mixtures of some pulmonary surfactant components. J Lipid Res 21:10–22
18. Minkov I, Mircheva K, Grozev N, Ivanova Tz I, Panaiotov I (2013) Properties of mixed monolayers of clinical lung surfactant, serum albumin and hydtophilic polymers. Colloids Surf B: Biointerfaces 101:135–142
19. Pandey R, Sharma S, Khuller GK (2004) Nebulization of liposome encapsulated antitubercular drugs in guinea pigs. Int J Antimicrob Agents 24:93–94
20. Van Klinken BJW, Dekker J, Buller HA (1995) Mucin gene structure and expression: protection vs. adhesion. Am J Physiol 32:G613–627
21. Groo AC, Gravier J, Saulnier P, Ailhas C, Benoit JP, Lagarce F (2012) Communication in conference "colloids and nanomedicine." Amsterdam, Netherlands
22. Gu M, Yildiz H, Carrier R, Belfort G (2013) Discovery of low mucus adhesion surfaces. Acta Biomater 9:5201–5207
23. Li X, Chen D, Le C, Zhu C, Gan Y, Hovgaard L, Yang M (2011) Novel mucus-penetrating liposomes as a potential oral drug delivery system: preparation, in vitro characterization, and enhanced cellular uptake. Int J Nanomedicine 6:3151–3162
24. Schulz M, Olubummoa A, Wolfgang H, Binder WH (2012) Beyond the lipid-bilayer: interaction of polymers and nanoparticles with membranes. Soft Matter 8:4849–4864
25. Vonarbourg A, Saulnier P, Passirani C, Benoit JP (2005) Electrokinetic properties of noncharged lipid nanocapsules: influence of the dipolar distribution at the interface. Electrophoresis 26:2066–2075
26. Yang T, Choi MK, Cui FD, Kim JS, Chung SJ, Shim CK, Kim DD (2007) Preparation and evaluation of paclitaxel-loaded PEGylated immunoliposome. J Control Release 120:169–177
27. Silva CA, Nobre TM, Pavinatto FJ, Oliveira ON Jr (2012) Interaction of chitosan and mucin in a biomembrane model environment. J Coll Int Sci 376:289–295
28. Galvez P, Bussieres S, Demers E, Salesse C (2009) Parameters modulating the maximum insertion pressure of proteins and peptides in lipid monolayers. Biochimie 91:718–733
29. McConnell HM (1991) Structures and transitions in lipid monolayers at the air–water interfaces. Annu Rev Phys Chem 42:171–195
30. Kaganer VM, Mohwald H, Dutta P (1999) Structure and phase transitions in Langmuir monolayers. Rev Mod Phys 71:779–819
31. Nielsen LK, Bjørnholm T, Mouritsen OG (2007) Thermodynamic and real-space structural evidence of a 2D critical point in phospholipid monolayer. Langmuir 23:11684–11692
32. Gudmand M (2008) Phase behavior and enzyme dynamics at the liquid–water interface-a monolayer, fluorescence microscopy, and spectroscopy study. PhD thesis, Nanoscience Center, University of Copenhagen, Denmark, pp 82–93
33. Stemmer A, Engel A (1990) Imaging biological macromolecules by STM: quantitative interpretation of topographs. Ultramicroscopy 34:129–140
34. Balashev K, Jensen TR, Kjaer K, Bjornholm T (2001) Novel methods for studying lipids and lipases and their mutual interaction at interfaces. Part I. Atomic force microscopy. Biochimie 83:387–397